Enhancement of superconductivity in thin films of Sn under high pressure

Misaki Sasaki,[1] Masahiro Ohkuma,[2,*] Ryo Matsumoto,[2] Toru Shinmei,[3] Tetsuo Irifune,[3] Yoshihiko Takano,[2] and Katsuya Shimizu[1]

[1]*KYOKUGEN, Graduate School of Engineering Science, Osaka University, Toyonaka 560-8531, Osaka, Japan*

[2]*Research Center for Materials Nanoarchitectonics (MANA), National Institute for Materials Science, Tsukuba 305-0047, Ibaraki, Japan*

[3]*Geodynamics Research Center, Ehime University, Matsuyama 790-8577, Ehime, Japan*

(Received 10 April 2024; revised 29 January 2025; accepted 17 March 2025; published 27 March 2025)

We investigated the pressure effects of superconductivity on thin films of Sn. The elemental superconductor Sn with a body-centered-tetragonal structure, β-Sn, exhibits superconductivity below the superconducting transition temperature ($T_c = 3.72$ K) at ambient pressure. T_c of Sn increases with lowering dimension such as in thin-film and nanowire growth, or by high-pressure application. For thin films, T_c exhibits a slight increase up to approximately 4 K compared to the bulk value, attributable to the crystalline size and lattice disorder. By applying pressure on a bulk Sn, T_c initially decreases from 3.72 K as the pressure increases. Further increasing pressure up to 10 GPa, T_c increases to 5.3 K with the structural transformation. However, the combination of these effects on thin films of Sn, namely, thin-film growth and pressure effects, remains underexplored. In this paper, we combined film-growth and pressure-application techniques to further increase T_c using a diamond anvil cell with boron-doped diamond electrodes. The drop of electrical resistance suggesting the onset of T_c on the thin film reached above 6 K in the γ-Sn phase. Further, the upper critical magnetic field was drastically enhanced. Atomic force microscopy suggests that the refinement of the grain size of the thin film under nonhydrostatic pressure conditions contributes to stabilizing the higher T_c of γ-Sn.

DOI: 10.1103/PhysRevB.111.104513

I. INTRODUCTION

Applying high pressure to directly compress a material is a useful approach to investigate intriguing physical properties and search for new materials [1,2]. For instance, oxygen—a gas at ambient conditions— exhibits metallic behaviors and superconductivity at high pressures [3,4]. Recently, high-temperature superconductors such as hydrogen-rich materials and nickelates under high pressure have attracted considerable attention [5–18]. In addition, recent discoveries of high-temperature superconducting states in elemental solid Ti and Sc at extreme pressures imply the potential of high-temperature superconductivity in the high-pressure phases of other elements [19–21].

Some elemental superconductors with thin-film dimensions show an increase in superconducting transition temperature (T_c) compared to the bulk value, attributable to the crystalline size and lattice disorder [22–25]. In the case of Sn, T_c for thin films and nanowires varies slightly depending on the size and surface morphology [26–29]. The mechanism of T_c enhancement is not thoroughly clear although it has been proposed to arise from changes in the phonon density of states, the electron density of states, and the electron-phonon coupling [30–32].

Sn exhibits various crystal structures at high pressures [33–35]. Half a century ago, Wittig investigated the electrical transport properties of bulk Sn at high pressures of up to 16 GPa and revealed the highest T_c is 5.3 K at 11.3 GPa on the pressure-induced phase, γ-Sn, where β-Sn shows superconductivity below 3.72 K at ambient pressure [36]. However, research on the combination of pressure application and thin-film growth on elemental superconductors is inadequate. Here, we hypothesize that changing the crystalline size of a thin film via pressure application could stabilize the higher T_c.

In this paper, we combined thin-film growth and pressure-application techniques to increase T_c using a diamond anvil cell (DAC) with boron-doped diamond (BDD) electrodes [37–39]. We investigated the pressure effects on the superconductivity of thin films of Sn compared to the bulk sample. We observed a higher T_c for the thin film compared to previous studies on the high-pressure phase. Further, we observed a drastically enhanced critical magnetic field on the thin film under high pressure.

II. EXPERIMENTAL PROCEDURE

Thin films of Sn were deposited on a diamond anvil by resistance heating evaporation. The target metal was high-purity Sn, purchased from Kojundo Chemical Laboratory Company, Ltd. Comparing with the high-pressure measurements, we also prepared Sn thin films on a diamond substrate for electrical transport measurements at ambient pressure. The film deposition on the two diamonds was performed simultaneously. The optical images of the thin films on the diamond anvil and the diamond substrate are shown in Fig. 1(a) and the

*Present address: School of Engineering, Institute of Science Tokyo, Yokohama, Kanagawa 226-8501, Japan.

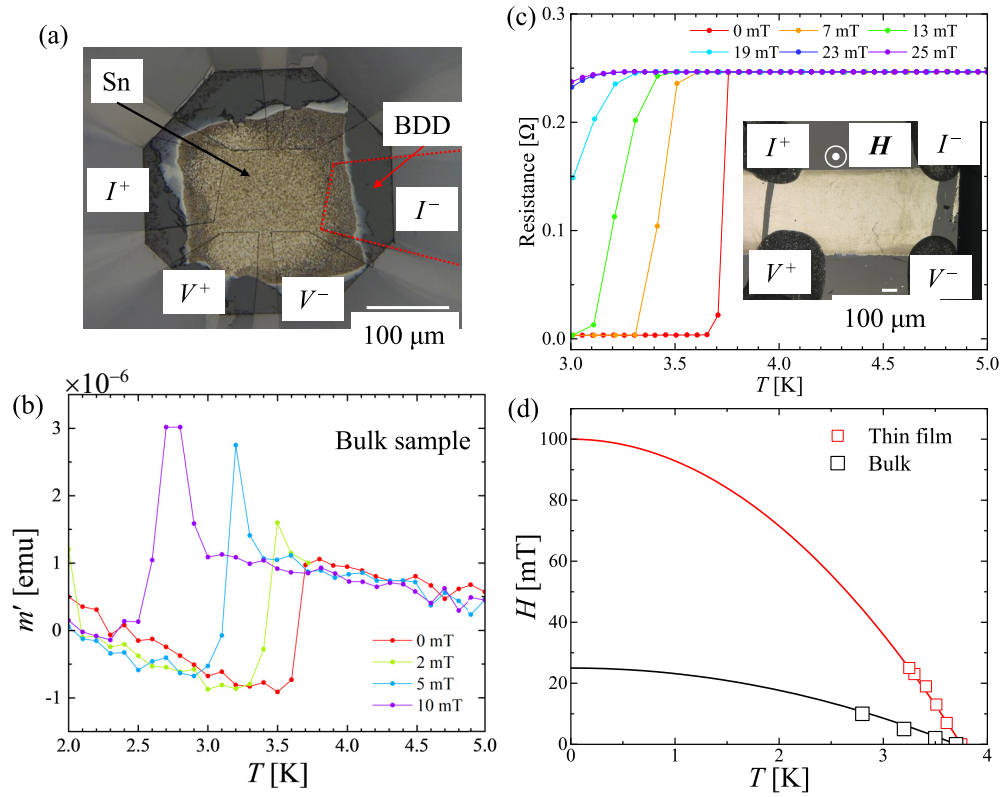

FIG. 1. (a) Optical image of a thin film of Sn on a diamond anvil with BDD electrodes. The dotted area indicates one of the BDD electrodes. (b) T dependence of the in-phase component of m' on the bulk Sn. (c) T dependence of R on a thin film of Sn on a diamond substrate. The magnetic field was applied perpendicularly to the film. The inset shows the optical image of a thin film of Sn on a diamond substrate. The thickness of the thin film was approximately 100 nm. (d) T dependence of the critical magnetic field on the thin film and bulk Sn.

inset of Fig. 1(c), respectively. The film thickness and surface morphology of the films were evaluated via atomic force microscopy (AFM; Nanocute, SII NanoTechnology, Inc.) at room temperature. For the magnetic measurements of the bulk Sn, a wire of high-purity Sn (Nilaco Corporation) was used.

High-pressure generation was performed using DAC. The pressure value at room temperature was evaluated using ruby fluorescence and the Raman shift of diamond [40,41]. In the electrical transport measurements, a diamond anvil with BDD electrodes with a culet size of 300 μm was used [37–39]. The BDD electrodes were deposited homoepitaxially on the diamond anvil by microwave plasma chemical vapor deposition [42]. This electrode exhibits high durability and can be reused until the diamond anvil itself fractures. Further, thin films could be deposited directly on the diamond anvil with BDD electrodes, eliminating the need for an electrode fabrication process after thin-film deposition [37,43,44]. The pressure-transmitting media in the solid, liquid, and gaseous states are compatible with this system. A gasket of stainless steel was preindented and a 200-μm-diameter hole was drilled. The insulating layer was prepared using a MgO-epoxy mixture. We termed this setup as nonhydrostatic. We also performed high-pressure generation with a better hydrostatic pressure condition than the nonhydrostatic measurement using glycerol as the liquid pressure-transmitting medium. A 150-μm-diameter hole was drilled in the insulating layer of the MgO-epoxy mixture to prepare the sample space, which was filled with glycerol. We termed this setup as quasihydrostatic. In quasihydrostatic pressure measurements, the pressure value was evaluated using the Raman shift of diamond [41]. The electrical transports under a magnetic field (H) perpendicular to the surface were measured by a four-terminal method by a physical properties measurement system (Quantum Design).

For magnetic measurements, we used a miniature DAC in combination with a superconducting quantum interference device magnetometer (MPMS, Quantum Design) [45–50]. A nanopolycrystalline diamond with culet size of 600 μm and a preindented tungsten gasket with a hole size of 200 μm were used [51]. Bulk Sn pieces and ruby powders were loaded into the sample space without a pressure-transmitting medium. The in-phase component of the ac magnetic response (m') was measured. The frequency and amplitude of the ac field were 3 Hz and 0.2 mT, respectively.

III. EXPERIMENTAL RESULTS

A. Ambient pressure

Figure 1(b) shows the temperature (T) dependence of m' for the bulk Sn under H, where no background signal from DAC is subtracted. Below 3.7 K, a diamagnetic signal suggesting a superconducting state was observed at $H = 0$. The T_c onset was decreased by applying H. Figure 1(c) shows the T dependence of the electrical resistance (R) under H perpendicular to the film surface. The residual resistance ratio (RRR) was estimated to be 11. At $H = 0$, an R drop suggesting the

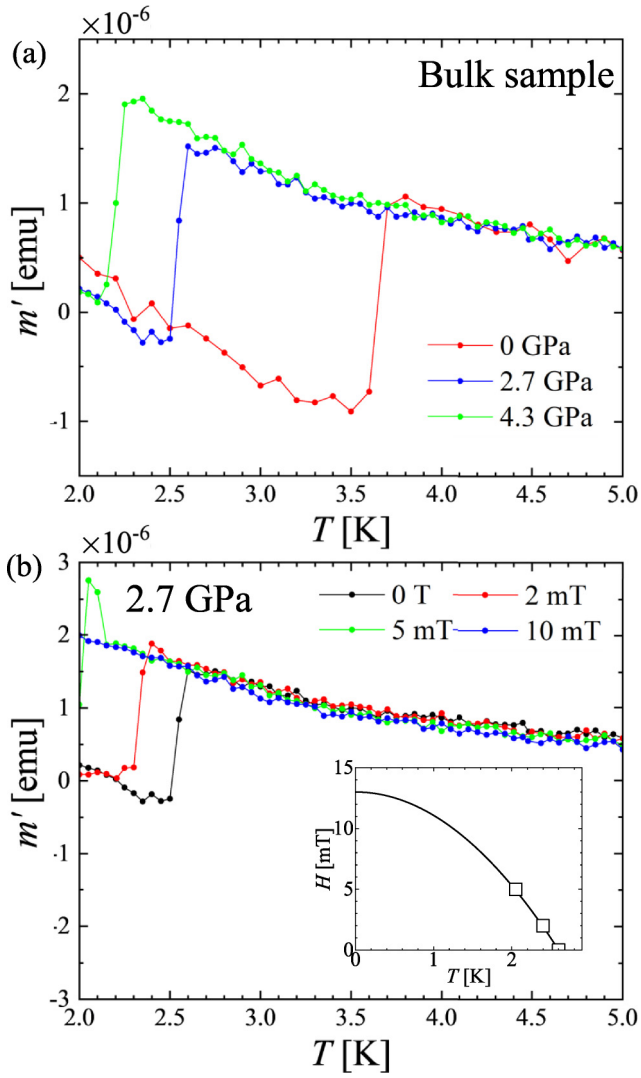

FIG. 2. (a) T dependence of m' on bulk Sn under high pressures. (b) T dependence of m' at 2.7 GPa under varying magnetic fields. The inset shows the T dependence of the critical magnetic field.

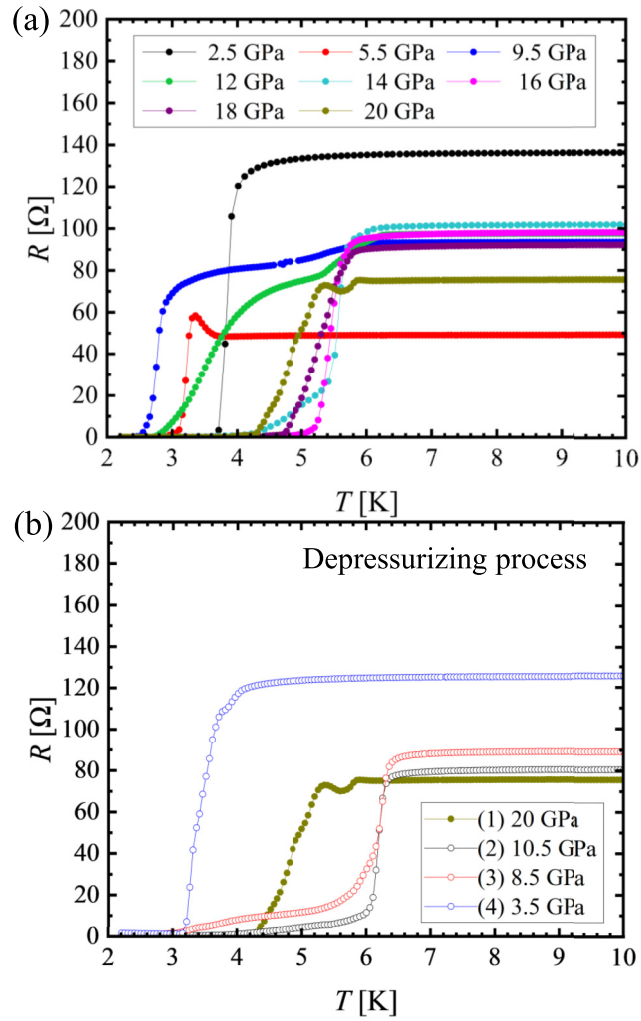

FIG. 3. T dependence of electrical R under nonhydrostatic pressure with a (a) pressurizing process and (b) depressurizing process. The number in (b) indicates the order of measurements.

onset of a superconducting transition was observed at 3.75 K. T_c slightly increased compared to the bulk value and was similar to values from previous studies on thin films [27,28]. By applying H, the onset of T_c decreased with increasing H. However, the critical magnetic field was three times higher than that of the bulk Sn [Fig. 1(d)]. An H_c of 100 mT estimated using $H_c(T) = H_c[1 - (T/T_c)^2]$ was similar to that of a previous study [28]. Considering H_c, the thin film transformed into a type-II superconductor, as previously reported [28,52,53].

B. Nonhydrostatic pressure on bulk Sn

Figure 2(a) shows the T dependence of m' on the bulk Sn under high pressures. On applying pressure, T_c decreased, as previously reported. Figure 2(b) shows the T dependence of m' at 2.7 GPa under varying H. A decrease of T_c was observed by applying $H = 2$ mT. At $H = 10$ mT, T_c was below 2 K. H_c was evaluated to be 13 mT, as shown in the inset of Fig. 2(b).

C. Nonhydrostatic pressure on thin film

Figure 3(a) shows the T dependence of R on a thin film of Sn under high pressures on pressurization. As shown in the inset of Fig. 4(a), RRR was estimated to be 1.4 at 2.5 GPa, which was much lower than that under ambient pressure. We speculate that the crystallographic defect was introduced because of the nonhydrostatic pressure condition. A R drop suggesting the superconducting transition was observed around 4 K, whereas T_c was 3.75 K under ambient pressure. T_c decreased on further increasing the pressure, as previously reported. R showed peak behavior just above T_c at 5.5 GPa, possibly due to the granularity or disorder on the thin films. Above 9.5 GPa, R tended to slightly decrease around 6 K, suggesting the superconducting transition, where the γ-Sn phase could emerge. With further pressure application, the R drop became significant, and T_c slightly decreased. After applying 20 GPa, the pressure was decreased to 10.5 GPa. Figure 3(b) shows the T dependence of R for a thin film of Sn under high pressures with depressurization. The onset of T_c increased to 6.3 K at 10.5 GPa, and γ-Sn remained at 8.5 GPa. γ-Sn vanished when the pressure was decreased to 3.5 GPa.

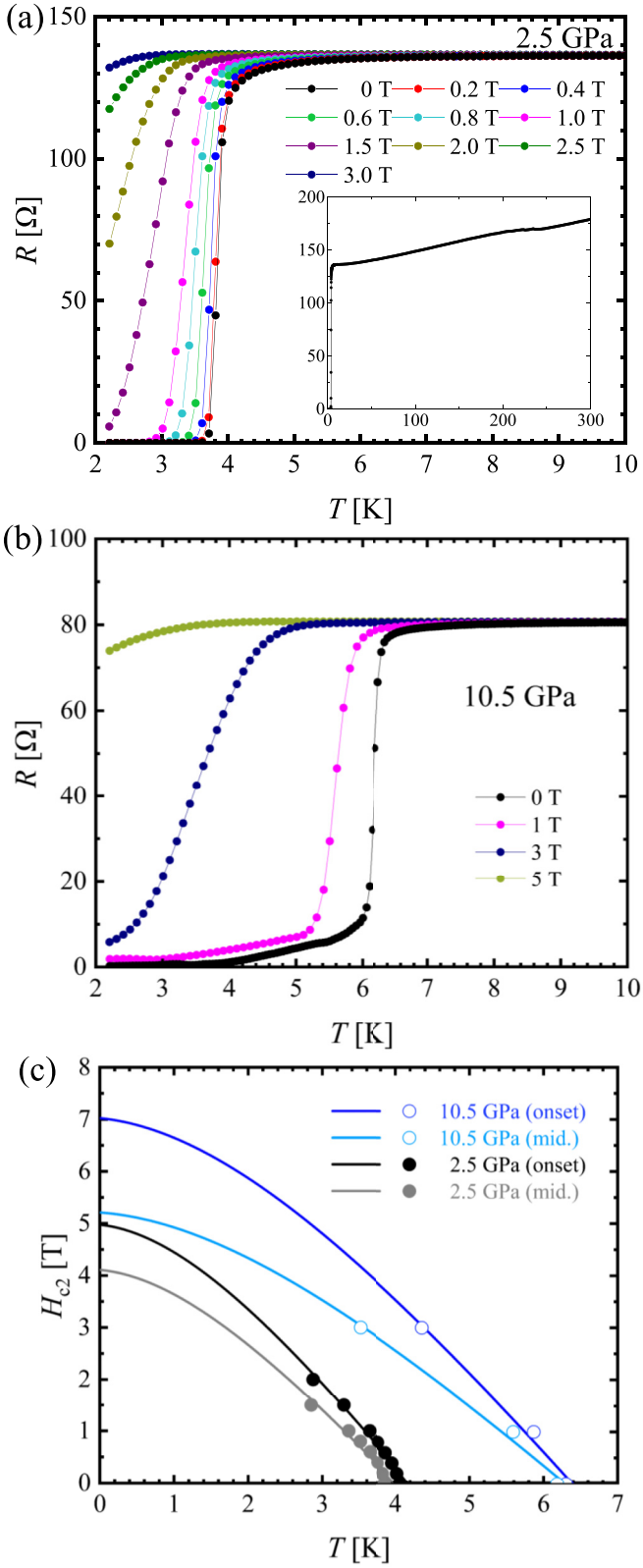

FIG. 4. (a) and (b) T dependence of R under a magnetic field at (a) 2.5 and (b) 10.5 GPa. The inset of (a) shows T dependence of R between 2 and 300 K at 2.5 GPa without an external magnetic field. (c) T dependence of the upper critical magnetic field at 2.5 and 10.5 GPa. The solid lines represent the fitting curves estimated by the WHH model.

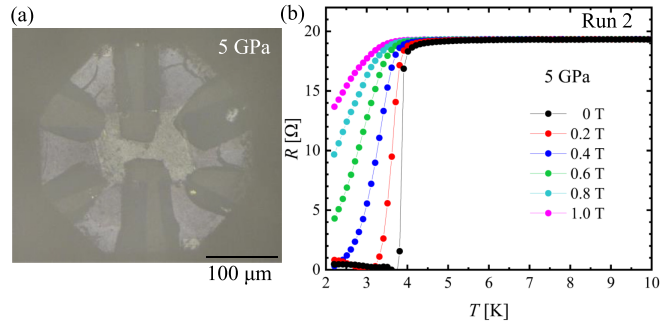

FIG. 5. (a) Optical image of a thin film of Sn at 5 GPa and (b) T dependence of R at 5 GPa.

Figures 4(a) and 4(b) show the T dependence of R for a thin film of Sn under various H at 2.5 and 10.5 GPa under the nonhydrostatic pressure condition. T_c was observed at 1 T, whereas the upper critical magnetic field (H_{c2}) was approximately 0.1 T under ambient pressure. A drastic H_{c2} enhancement was also observed in the γ phase at 10.5 GPa. As shown in Fig. 4(c), H_{c2} estimated using the Werthamer-Helfand-Hohenberg (WHH) model reached several teslas at high pressures [54–56]. Notably, the H_{c2} enhancement of β-Sn under the nonhydrostatic pressure condition was observed reproducibly. Figure 5(b) shows the T dependence of R for a thin film of Sn with the other setup at 5 GPa. The optical image of a thin film of Sn is shown in Fig. 5(a). A decrease in R suggesting the superconducting transition was observed even at $H = 1.0$ T.

There are two possible scenarios for the H_{c2} enhancement. The first is the enhancement of the flux-pinning force. The crystallographic defects introduced by nonhydrostatic pressure could serve as pinning centers, potentially leading to an increase in H_{c2}. The other is the shortening of the mean free path of the electrons and the resulting shortening of the coherence length. Considering that the thickness of the thin film was approximately 100 nm, the electrical resistivity of the normal state near T_c was estimated to be approximately 2.5 μΩ cm for the ambient pressure measurement. This value is consistent with those reported in previous studies [28,53]. In contrast, the electrical resistivities of the thin films for 2.5 GPa of run 1 and 5 GPa of run 2 were approximately 1.7×10^3 and 81 μΩ cm, respectively. The increase in the electrical resistivity near T_c suggests that the mean free path of the electrons is shortened by the application of pressure.

D. Quasihydrostatic pressure on thin film

We performed high-pressure generation with a better hydrostatic pressure condition using glycerol as the liquid pressure transmitted medium. Figure 6(a) shows the R-T of the thin film at 9 GPa under quasihydrostatic pressure conditions. The optical image of the thin film inside the DAC is shown in the inset of Fig. 6(a). The RRR was within 2–3 in quasihydrostatic pressure measurements, which was slightly higher than those for the nonhydrostatic pressure condition. An R drop suggesting a superconducting transition was observed around 5 K. Figure 6(b) shows R-T under a

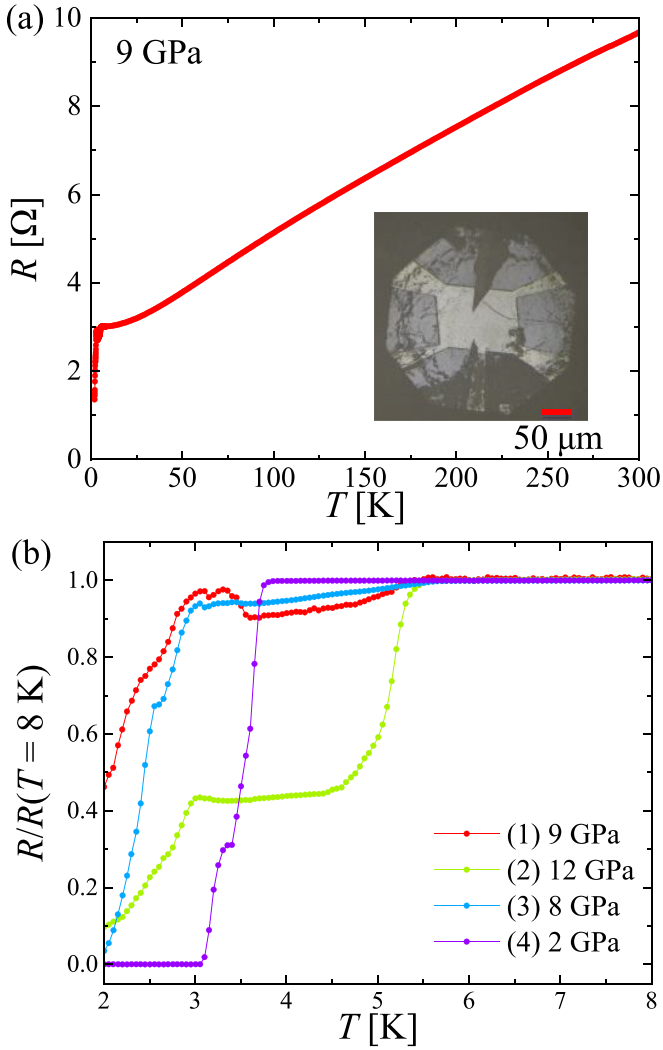

FIG. 6. (a) T dependence of R at 9 GPa. The inset shows the optical image of the thin film. (b) T dependence of R under high pressures between 2 and 8 K.

quasihydrostatic pressure condition between 2 and 8 K with the warming process. The R value was normalized using the value at 8 K. At 9 GPa, R slightly decreased with decreasing T around 5.3 K, suggesting the superconducting transition on γ-Sn. An R drop was also observed around 3 K. The γ-Sn phase became significant on further pressure application. The onset of T_c slightly increased at 12 GPa. We also decreased the pressure from 12 to 8 GPa. A decrease of R suggesting the superconducting transition of γ-Sn was slightly observed, whereas γ-Sn was clearly observed at 8.5 GPa under the nonhydrostatic pressure condition. With a further pressure decrease, γ-Sn vanished at 2 GPa.

IV. DISCUSSION

A. Pressure dependence of T_c

Figure 7 shows the pressure dependence of T_c for the thin film and bulk samples compared with results from a previous study [36]. For the bulk Sn, the behavior of T_c with respect to pressure was in good agreement with the previous study. A

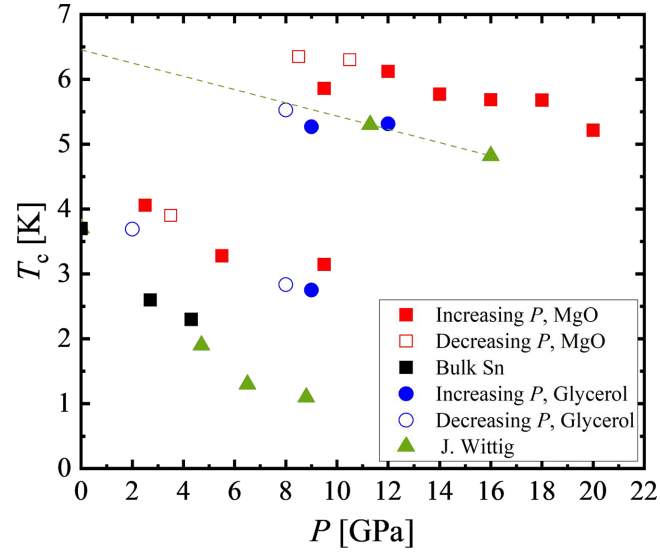

FIG. 7. Pressure dependence of the superconducting transition temperature. The green triangles indicate the results by Wittig [36]. The dotted line indicates a guide for the eyes.

similar tendency was observed for the thin film in the β-Sn phase, however, its T_c was higher compared to bulk Sn. One possible reason is the geometry of the thin film. As shown in Fig. 1(a), the thin-film area occupies approximately 70% of the culet of the diamond anvil, which produces the pressure distribution. In the γ-Sn phase, T_c with quasihydrostatic pressure measurements showed a trend similar to previous results [36]. Meanwhile, T_c with nonhydrostatic pressure showed a higher value. We observed the highest T_c of 6.3 K at 10.5 GPa, which was approximately 10% higher than that reported in a previous study [36]. The highest T_c is not fully explained by the pressure gradient. Assuming that the T_c of bulk γ-Sn continues to change at a rate of -0.11 K/GPa, it is necessary to decrease the pressure to 4 GPa from the γ phase above 10 GPa. However, the γ phase cannot exist metastably under this pressure as was observed during the γ to β phase transition on the decompression process [Fig. 3(b)]. We emphasize that we observed the midpoint of T_c to be greater than 6.0 K [Fig. 4(b)].

B. Atomic force microscopy

To investigate the morphology on the thin films, we performed AFM measurements before and after applying pressure under the nonhydrostatic pressure condition. Figures 8(a) and 8(b) show the optical and AFM images of the thin film before pressurization. The thin film of Sn was deposited on a diamond anvil without BDD electrodes. The average film thickness was evaluated to be 70 nm. A magnified AFM image is shown in Fig. 8(c). The average grain size was estimated to be approximately 300 nm. Figure 8(d) shows the optical image of the thin film after applying pressure up to 4.2 GPa. The pressure was evaluated by the diamond Raman shift. Most of the thin film was peeled off and transferred to the MgO-epoxy mixture. We measured the small remaining thin-film area. Figure 8(e) shows the AFM image of the thin film after pressurization.

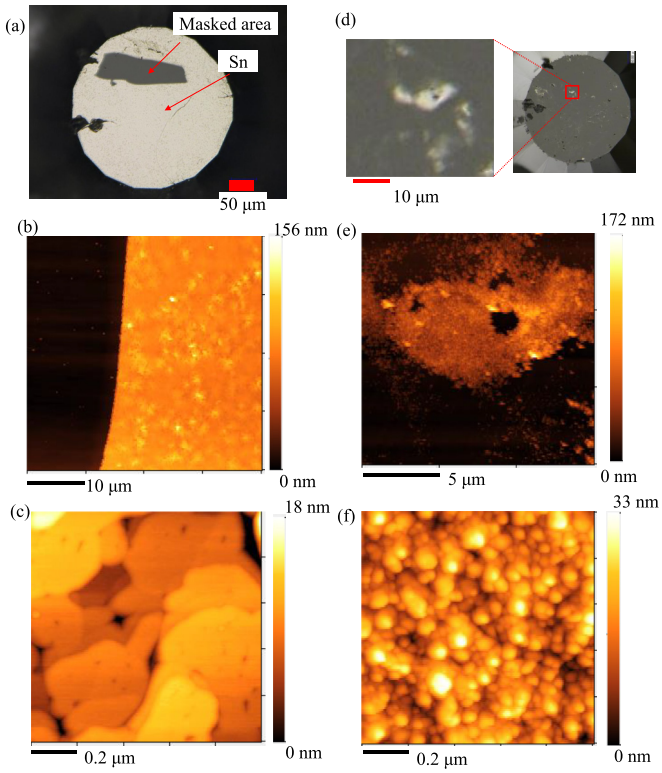

FIG. 8. (a) Optical image of the thin film of Sn on a diamond anvil before pressurization. (b) and (c) AFM image on the thin film before pressurization. (d) Optical images of the thin film of Sn on the diamond anvil after pressurization. (e) and (f) AFM image of the thin film after pressurization.

The average film thickness was evaluated to be 60 nm. A magnified view is shown in Fig. 8(f). The grain size was reduced to several tens of nanometers on pressure application.

Next, we performed AFM measurements under a quasihydrostatic pressure condition for comparison with the nonhydrostatic pressure measurements. The thin film was the same as that used in the *R-T* measurement. Figures 9(a) and 9(b) show the AFM images of the thin film before applying pressure. The average thickness and average grain size were evaluated to be 82 and 600 nm, respectively. Figures 9(c) and 9(d) show the AFM images on the thin film after applying pressure up to 12 GPa. The pressure-transmitting medium was removed using ethanol and nitrogen gas. The average thickness was evaluated to be 91 nm. Unlike the nonhydrostatic pressure measurements, grain refinement was not observed.

The AFM results revealed that the grain refinement was observed only under the nonhydrostatic pressure condition. In the *R-T* results, the maximum T_c value under the nonhydrostatic condition was 10% higher than that under the quasihydrostatic condition, suggesting that grain refinement plays a pivotal role in stabilizing the higher T_c. Smaller grain sizes tend to have higher T_c, because of phonon softening under ambient pressure [32]. Houben *et al.* performed nuclear resonant inelastic x-ray scattering on nanostructured films and bulk Sn to investigate the phonon density of states and observed a decrease in the high-energy phonon modes and a slight increase in the low-energy phonon modes in

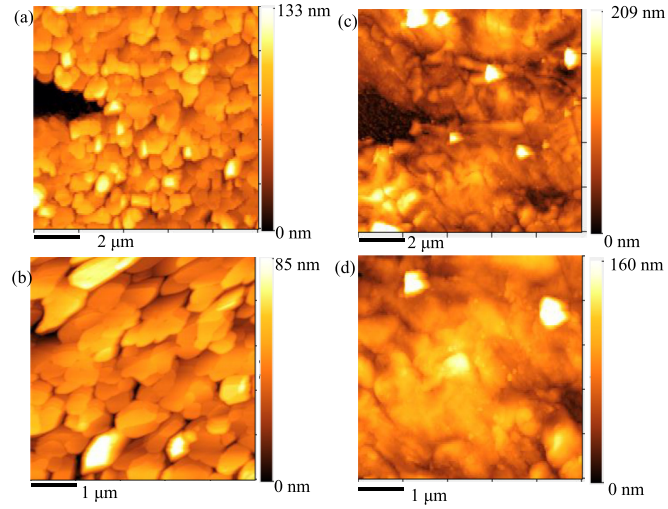

FIG. 9. AFM under quasihydrostatic pressure condition. (a) and (b) AFM image of the thin film before pressurization. (c) and (d) AFM image of the thin film after pressurization.

nanostructured films [31,32]. Using the obtained phonon spectra, calculations based on the Allen-Dynes-McMillan formalism yielded T_c values in good agreement with the experimental data. In nanostructured films, the electron-phonon coupling increased by up to 10%, suggesting that phonon softening and the associated change in electron-phonon coupling play a major role in the T_c increase. We consider that the T_c increase under the nonhydrostatic pressure condition is related to the grain size and that grain refinement could induce changes in the electron-phonon coupling.

C. Possible higher T_c on Sn

Recently, anomalies in magnetization, resistance, and heat capacity suggesting the superconducting transition were observed around 5.5 K in nanowires of Sn [57]. Further, based

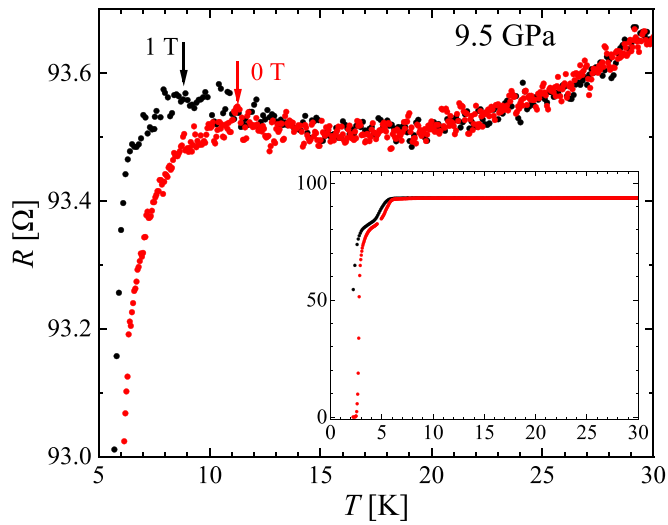

FIG. 10. Temperature dependence of the electrical resistance at 9.5 GPa. The downward arrows indicate the onset of the anomalies in the resistance.

on scanning tunneling microscopy, a thin film of Sn deposited on the $SrTiO_3$ substrate exhibited superconductivity around 8 K [58]. Indeed, in our thin film, a decrease of R was observed at 11 K under 9.5 GPa, suggesting the signature of the superconducting transition, and the anomaly shifted to lower T by applying the magnetic field (Fig. 10). On the other hand, some granular or amorphous thin films exhibit a decrease in resistance at higher T than T_c due to the effects of fluctuations [59–62]. Further investigations such as magnetic measurements [63,64], heat capacity measurements [65], and scanning tunneling microscopy [66] under high pressure may offer insights for the possible stabilization of higher T_c.

V. CONCLUSION

In conclusion, we demonstrated the pressure effect on the superconductivity of thin films of Sn. We observed superconductivity below 6.3 K in the γ phase of Sn, which was approximately 10% higher than previous bulk results. Further, the H_{c2} drastically increased under the nonhydrostatic high-pressure condition. We also observed the signature of the superconducting transition at higher T than T_c. AFM results suggest that the grain refinement under nonhydrostatic pressure contributes to the stabilization of the higher T_c of γ-Sn.

ACKNOWLEDGMENTS

This work was supported by JSPS KAKENHI Grants No. 19H02177 and No. 20H05644, and JST-Mirai Program Grant No. JPMJMI17A2. This work was also supported by the Joint Usage/Research Center PRIUS, Ehime University, Japan.

DATA AVAILABILITY

The data that support the findings of this article are openly available [67].

[1] H.-K. Mao, X.-J. Chen, Y. Ding, B. Li, and L. Wang, Solids, liquids, and gases under high pressure, Rev. Mod. Phys. **90**, 015007 (2018).

[2] S. Yamanaka, Silicon clathrates and carbon analogs: High pressure synthesis, structure, and superconductivity, Dalton Trans. **39**, 1901 (2010).

[3] K. Shimizu, K. Suhara, M. Ikumo, M. I. Eremets, and K. Amaya, Superconductivity in oxygen, Nature (London) **393**, 767 (1998).

[4] K. Shimizu, K. Amaya, and N. Suzuki, Pressure-induced superconductivity in elemental materials, J. Phys. Soc. Jpn. **74**, 1345 (2005).

[5] A. P. Drozdov, M. I. Eremets, I. A. Troyan, V. Ksenofontov, and S. I. Shylin, Conventional superconductivity at 203 Kelvin at high pressures in the sulfur hydride system, Nature (London) **525**, 73 (2015).

[6] A. P. Drozdov, P. P. Kong, V. S. Minkov, S. P. Besedin, M. A. Kuzovnikov, S. Mozaffari, L. Balicas, F. F. Balakirev, D. E. Graf, V. B. Prakapenka, E. Greenberg, D. A. Knyazev, M. Tkacz, and M. I. Eremets, Superconductivity at 250 K in lanthanum hydride under high pressures, Nature (London) **569**, 528 (2019).

[7] M. Somayazulu, M. Ahart, A. K. Mishra, Z. M. Geballe, M. Baldini, Y. Meng, V. V. Struzhkin, and R. J. Hemley, Evidence for superconductivity above 260 K in lanthanum superhydride at megabar pressures, Phys. Rev. Lett. **122**, 027001 (2019).

[8] R. Matsumoto, M. Einaga, S. Adachi, S. Yamamoto, T. Irifune, K. Terashima, H. Takeya, Y. Nakamoto, K. Shimizu, and Y. Takano, Electrical transport measurements for superconducting sulfur hydrides using boron-doped diamond electrodes on beveled diamond anvil, Supercond. Sci. Technol. **33**, 124005 (2020).

[9] D. V. Semenok, A. G. Kvashnin, A. G. Ivanova, V. Svitlyk, V. Y. Fominski, A. V. Sadakov, O. A. Sobolevskiy, V. M. Pudalov, I. A. Troyan, and A. R. Oganov, Superconductivity at 161 K in thorium hydride ThH_{10}: Synthesis and properties, Mater. Today **33**, 36 (2020).

[10] W. Chen, D. V. Semenok, X. Huang, H. Shu, X. Li, D. Duan, T. Cui, and A. R. Oganov, High-temperature superconducting phases in cerium superhydride with a T_c up to 115 K below a pressure of 1 megabar, Phys. Rev. Lett. **127**, 117001 (2021).

[11] P. Kong, V. S. Minkov, M. A. Kuzovnikov, A. P. Drozdov, S. P. Besedin, S. Mozaffari, L. Balicas, F. F. Balakirev, V. B. Prakapenka, S. Chariton, D. A. Knyazev, E. Greenberg, and M. I. Eremets, Superconductivity up to 243 K in the yttrium-hydrogen system under high pressure, Nat. Commun. **12**, 5075 (2021).

[12] I. A. Troyan, D. V. Semenok, A. G. Kvashnin, A. V. Sadakov, O. A. Sobolevskiy, V. M. Pudalov, A. G. Ivanova, V. B. Prakapenka, E. Greenberg, A. G. Gavriliuk, I. S. Lyubutin, V. V. Struzhkin, A. Bergara, I. Errea, R. Bianco, M. Calandra, F. Mauri, L. Monacelli, R. Akashi, and A. R. Oganov, Anomalous high-temperature superconductivity in YH_6, Adv. Mater. **33**, 2006832 (2021).

[13] Z. Li, X. He, C. Zhang, X. Wang, S. Zhang, Y. Jia, S. Feng, K. Lu, J. Zhao, J. Zhang, B. Min, Y. Long, R. Yu, L. Wang, M. Ye, Z. Zhang, V. Prakapenka, S. Chariton, P. A. Ginsberg, J. Bass *et al.*, Superconductivity above 200 K discovered in superhydrides of calcium, Nat. Commun. **13**, 2863 (2022).

[14] L. Ma, K. Wang, Y. Xie, X. Yang, Y. Wang, M. Zhou, H. Liu, X. Yu, Y. Zhao, H. Wang, G. Liu, and Y. Ma, High-temperature superconducting phase in clathrate calcium hydride CaH_6 up to 215 K at a pressure of 172 GPa, Phys. Rev. Lett. **128**, 167001 (2022).

[15] Y. Song, J. Bi, Y. Nakamoto, K. Shimizu, H. Liu, B. Zou, G. Liu, H. Wang, and Y. Ma, Stoichiometric ternary superhydride $LaBeH_8$ as a new template for high-temperature superconductivity at 110 K under 80 GPa, Phys. Rev. Lett. **130**, 266001 (2023).

[16] S. Cross, J. Buhot, A. Brooks, W. Thomas, A. Kleppe, O. Lord, and S. Friedemann, High-temperature superconductivity in La_4H_{23} below 100 GPa, Phys. Rev. B **109**, L020503 (2024).

[17] H. Sun, M. Huo, X. Hu, J. Li, Z. Liu, Y. Han, L. Tang, Z. Mao, P. Yang, B. Wang, J. Cheng, D.-X. Yao, G.-M. Zhang, and M. Wang, Signatures of superconductivity near 80 K in a nickelate under high pressure, Nature (London) **621**, 493 (2023).

[18] H. Sakakibara, M. Ochi, H. Nagata, Y. Ueki, H. Sakurai, R. Matsumoto, K. Terashima, K. Hirose, H. Ohta, M. Kato, Y. Takano, and K. Kuroki, Theoretical analysis on the possibility of superconductivity in the trilayer Ruddlesden-Popper nickelate $La_4Ni_3O_{10}$ under pressure and its experimental examination: Comparison with $La_3Ni_2O_7$, Phys. Rev. B **109**, 144511 (2024).

[19] X. Liu, P. Jiang, Y. Wang, M. Li, N. Li, Q. Zhang, Y. Wang, Y.-L. Li, and W. Yang, T_c up to 23.6 K and robust superconductivity in the transition metal δ-Ti phase at megabar pressure, Phys. Rev. B **105**, 224511 (2022).

[20] C. Zhang, X. He, C. Liu, Z. Li, K. Lu, S. Zhang, S. Feng, X. Wang, Y. Peng, Y. Long, R. Yu, L. Wang, V. Prakapenka, S. Chariton, Q. Li, H. Liu, C. Chen, and C. Jin, Record high T_c element superconductivity achieved in titanium, Nat. Commun. **13**, 5411 (2022).

[21] J. Ying, S. Liu, Q. Lu, X. Wen, Z. Gui, Y. Zhang, X. Wang, J. Sun, and X. Chen, Record high 36 K transition temperature to the superconducting state of elemental scandium at a pressure of 260 GPa, Phys. Rev. Lett. **130**, 256002 (2023).

[22] W. Buckel and R. Hilsch, Influence of condensation at low temperatures on electrical resistance and superconductivity for various metals, Z. Phys. **138**, 109 (1954).

[23] B. Abeles, R. W. Cohen, and G. W. Cullen, Enhancement of superconductivity in metal films, Phys. Rev. Lett. **17**, 632 (1966).

[24] J. W. Garland, K. H. Bennemann, and F. M. Mueller, Effect of lattice disorder on the superconducting transition temperature, Phys. Rev. Lett. **21**, 1315 (1968).

[25] M. Strongin, O. F. Kammerer, J. E. Crow, R. D. Parks, D. H. Douglass, and M. A. Jensen, Enhanced superconductivity in layered metallic films, Phys. Rev. Lett. **21**, 1320 (1968).

[26] M. Tian, J. Wang, J. S. Kurtz, Y. Liu, M. H. W. Chan, T. S. Mayer, and T. E. Mallouk, Dissipation in quasi-one-dimensional superconducting single-crystal Sn nanowires, Phys. Rev. B **71**, 104521 (2005).

[27] M. H. Beutel, N. G. Ebensperger, M. Thiemann, G. Untereiner, V. Fritz, M. Javaheri, J. Nägele, R. Rösslhuber, M. Dressel, and M. Scheffler, Microwave study of superconducting Sn films above and below percolation, Supercond. Sci. Technol. **29**, 085011 (2016).

[28] W. Bang, T. D. Morrison, K. D. D. Rathnayaka, I. F. Lyuksyutov, D. G. Naugle, and W. Teizer, Characterization of superconducting Sn thin films and their application to ferromagnet-superconductor hybrids, Thin Solid Films **676**, 138 (2019).

[29] D. P. Lozano, S. Couet, C. Petermann, G. Hamoir, J. K. Jochum, T. Picot, E. Menéndez, K. Houben, V. Joly, V. A. Antohe, M. Y. Hu, B. M. Leu, A. Alatas, A. H. Said, S. Roelants, B. Partoens, M. V. Milošević, F. M. Peeters, L. Piraux, J. V. de Vondel *et al.*, Experimental observation of electron-phonon coupling enhancement in Sn nanowires caused by phonon confinement effects, Phys. Rev. B **99**, 064512 (2019).

[30] K. Knorr and N. Barth, Superconductivity and phonon spectra of disordered thin films, Solid State Commun. **8**, 1085 (1970).

[31] K. Houben, S. Couet, M. Trekels, E. Menéndez, T. Peissker, J. W. Seo, M. Y. Hu, J. Y. Zhao, E. E. Alp, S. Roelants, B. Partoens, M. V. Milošević, F. M. Peeters, D. Bessas, S. A. Brown, A. Vantomme, K. Temst, and M. J. Van Bael, Lattice dynamics in Sn nanoislands and cluster-assembled films, Phys. Rev. B **95**, 155413 (2017).

[32] K. Houben, J. K. Jochum, S. Couet, E. Menéndez, T. Picot, M. Y. Hu, J. Y. Zhao, E. E. Alp, A. Vantomme, K. Temst, and M. J. Van Bael, The influence of phonon softening on the superconducting critical temperature of Sn nanostructures, Sci. Rep. **10**, 5729 (2020).

[33] J. D. Barnett, V. E. Bean, and H. T. Hall, X-ray diffraction studies on tin to 100 Kilobars, J. Appl. Phys. **37**, 875 (1966).

[34] A. Salamat, R. Briggs, P. Bouvier, S. Petitgirard, A. Dewaele, M. E. Cutler, F. Corà, D. Daisenberger, G. Garbarino, and P. F. McMillan, High-pressure structural transformations of Sn up to 138 GPa: Angle-dispersive synchrotron x-ray diffraction study, Phys. Rev. B **88**, 104104 (2013).

[35] G. Deffrennes, P. Faure, F. Bottin, J.-M. Joubert, and B. Oudot, Tin (Sn) at high pressure: Review, X-ray diffraction, DFT calculations, and Gibbs energy modeling, J. Alloys Compd. **919**, 165675 (2022).

[36] J. Wittig, The superconductivity of tin and lead under very high pressure, Z. Phys. **195**, 228 (1966).

[37] R. Matsumoto, Y. Sasama, M. Fujioka, T. Irifune, M. Tanaka, T. Yamaguchi, H. Takeya, and Y. Takano, Note: Novel diamond anvil cell for electrical measurements using boron-doped metallic diamond electrodes, Rev. Sci. Instrum. **87**, 076103 (2016).

[38] R. Matsumoto, T. Irifune, M. Tanaka, H. Takeya, and Y. Takano, Diamond anvil cell using metallic diamond electrodes, Jpn. J. Appl. Phys. **56**, 05FC01 (2017).

[39] R. Matsumoto, A. Yamashita, H. Hara, T. Irifune, S. Adachi, H. Takeya, and Y. Takano, Diamond anvil cells using boron-doped diamond electrodes covered with undoped diamond insulating layer, Appl. Phys. Express **11**, 053101 (2018).

[40] H. K. Mao, P. M. Bell, J. W. Shaner, and D. J. Steinberg, Specific volume measurements of Cu, Mo, Pd, and Ag and calibration of the ruby R1 fluorescence pressure gauge from 0.06 to 1 Mbar, J. Appl. Phys. **49**, 3276 (1978).

[41] Y. Akahama and H. Kawamura, High-pressure Raman spectroscopy of diamond anvils to 250 GPa: Method for pressure determination in the multimegabar pressure range, J. Appl. Phys. **96**, 3748 (2004).

[42] Y. Takano, M. Nagao, I. Sakaguchi, M. Tachiki, T. Hatano, K. Kobayashi, H. Umezawa, and H. Kawarada, Superconductivity in diamond thin films well above liquid helium temperature, Appl. Phys. Lett. **85**, 2851 (2004).

[43] S. Adachi, R. Matsumoto, S. Yamamoto, T. D. Yamamoto, K. Terashima, Y. Saito, M. E. Echevarria, P. B. de Castro, P. Song, S. Iwasaki, H. Takeya, and Y. Takano, Demonstration of electric double layer gating under high pressure by the development of field-effect diamond anvil cell, Appl. Phys. Lett. **116**, 223506 (2020).

[44] R. Matsumoto, S. Nakano, S. Yamamoto, and Y. Takano, Synthesis and electrical transport measurement of superconducting hydrides using diamond anvil cell with boron-doped diamond electrodes, Jpn. J. Appl. Phys. **60**, 090902 (2021).

[45] M. Mito, M. Hitaka, T. Kawae, K. Takeda, T. Kitai, and N. Toyoshima, Development of miniature diamond anvil cell for the superconducting quantum interference device magnetometer, Jpn. J. Appl. Phys. **40**, 6641 (2001).

[46] M. Mito, T. Imakyurei, H. Deguchi, K. Matsumoto, H. Hara, T. Ozaki, H. Takeya, and Y. Takano, Effective disappearance of the Meissner signal in the cuprate superconductor

$YBa_2Cu_4O_8$ under uniaxial strain, J. Phys. Soc. Jpn. **83**, 023705 (2014).

[47] M. Mito, H. Goto, H. Matsui, H. Deguchi, K. Matsumoto, H. Hara, T. Ozaki, H. Takeya, and Y. Takano, Uniaxial strain effects on superconducting transition in $Y_{0.98}Ca_{0.02}Ba_2Cu_4O_8$, J. Phys. Soc. Jpn. **85**, 024711 (2016).

[48] M. Mito, K. Ogata, H. Goto, K. Tsuruta, K. Nakamura, H. Deguchi, T. Horide, K. Matsumoto, T. Tajiri, H. Hara, T. Ozaki, H. Takeya, and Y. Takano, Uniaxial strain effects on the superconducting transition in Re-doped Hg-1223 cuprate superconductors, Phys. Rev. B **95**, 064503 (2017).

[49] M. Abdel-Hafiez, Y. Zhao, Z. Huang, C.-w. Cho, C. H. Wong, A. Hassen, M. Ohkuma, Y.-W. Fang, B.-J. Pan, Z.-A. Ren, A. Sadakov, A. Usoltsev, V. Pudalov, M. Mito, R. Lortz, C. Krellner, and W. Yang, High-pressure effects on isotropic superconductivity in the iron-free layered pnictide superconductor $BaPd_2As_2$, Phys. Rev. B **97**, 134508 (2018).

[50] M. Mito, Y. Kitamura, T. Tajiri, K. Nakamura, R. Shiraishi, K. Ogata, H. Deguchi, T. Yamaguchi, N. Takeshita, T. Nishizaki, K. Edalati, and Z. Horita, Hydrostatic pressure effects on superconducting transition of nanostructured niobium highly strained by high-pressure torsion, J. Appl. Phys. **125**, 125901 (2019).

[51] T. Irifune, A. Kurio, S. Sakamoto, T. Inoue, and H. Sumiya, Ultrahard polycrystalline diamond from graphite, Nature (London) **421**, 599 (2003).

[52] G. J. Dolan and J. Silcox, Critical thicknesses in superconducting thin films, Phys. Rev. Lett. **30**, 603 (1973).

[53] M. Ohkuma, R. Matsumoto, and Y. Takano, Nonreciprocal supercurrent in thin film of type II superconducting Sn, Appl. Phys. Express **16**, 043004 (2023).

[54] E. Helfand and N. R. Werthamer, Temperature and purity dependence of the superconducting critical field, H_{c2}. II, Phys. Rev. **147**, 288 (1966).

[55] N. R. Werthamer, E. Helfand, and P. C. Hohenberg, Temperature and purity dependence of the superconducting critical field, H_{c2}. III. Electron spin and spin-orbit effects, Phys. Rev. **147**, 295 (1966).

[56] T. Baumgartner, M. Eisterer, H. W. Weber, R. Flükiger, C. Scheuerlein, and L. Bottura, Effects of neutron irradiation on pinning force scaling in state-of-the-art Nb_3Sn wires, Supercond. Sci. Technol. **27**, 015005 (2014).

[57] Y. Zhang, C. H. Wong, J. Shen, S. T. Sze, B. Zhang, H. Zhang, Y. Dong, H. Xu, Z. Yan, Y. Li, X. Hu, and R. Lortz, Dramatic enhancement of superconductivity in single-crystalline nanowire arrays of Sn, Sci. Rep. **6**, 32963 (2016).

[58] Z. Shao, Z. Zhang, H. Yuan, H. Sun, Y. Cao, X. Zhang, S. Li, H. Gedeon, T. Xiang, Q.-K. Xue, and M. Pan, Scanning tunneling microscopic observation of enhanced superconductivity in epitaxial Sn islands grown on $SrTiO_3$ substrate, Sci. Bull. **63**, 1332 (2018).

[59] R. E. Glover, Ideal resistive transition of a superconductor, Phys. Lett. A **25**, 542 (1967).

[60] L. G. Aslamasov and A. I. Larkin, The influence of fluctuation pairing of electrons on the conductivity of normal metal, Phys. Lett. A **26**, 238 (1968).

[61] W. J. Skocpol and M. Tinkham, Fluctuations near superconducting phase transitions, Rep. Prog. Phys. **38**, 1049 (1975).

[62] D. Sóñora, C. Carballeira, J. J. Ponte, F. Vidal, T. Grenet, and J. Mosqueira, Paraconductivity of granular Al films at high reduced temperatures and magnetic fields, Phys. Rev. B **100**, 104509 (2019).

[63] S. Hsieh, P. Bhattacharyya, C. Zu, T. Mittiga, T. J. Smart, F. Machado, B. Kobrin, T. O. Höhn, N. Z. Rui, M. Kamrani, S. Chatterjee, S. Choi, M. Zaletel, V. V. Struzhkin, J. E. Moore, V. I. Levitas, R. Jeanloz, and N. Y. Yao, Imaging stress and magnetism at high pressures using a nanoscale quantum sensor, Science **366**, 1349 (2019).

[64] M. Lesik, T. Plisson, L. Toraille, J. Renaud, F. Occelli, M. Schmidt, O. Salord, A. Delobbe, T. Debuisschert, L. Rondin, P. Loubeyre, and J.-F. Roch, Magnetic measurements on micrometer-sized samples under high pressure using designed NV centers, Science **366**, 1359 (2019).

[65] K. Umeo, Alternating current calorimeter for specific heat capacity measurements at temperatures below 10 K and pressures up to 10 GPa, Rev. Sci. Instrum. **87**, 063901 (2016).

[66] Z.-Y. Cao, H. Jang, S. Choi, J. Kim, S. Kim, J.-B. Zhang, A. S. Sharbirin, J. Kim, and T. Park, Spectroscopic evidence for the superconductivity of elemental metal Y under pressure, NPG Asia Mater. **15**, 5 (2023).

[67] M. Sasaki, M. Ohkuma, R. Matsumoto, T. Shinmei, T. Irifune, Y. Takano, and K. Shimizu, Enhancement of superconductivity on thin film of Sn under high pressure, Zenodo (2025), https://zenodo.org/records/14759622.